Applied Clay Science 216 (2022) 106365

Contents lists available at ScienceDirect

Applied Clay Science

journal homepage: www.elsevier.com/locate/clay

# Controlled silica core removal from $SiO_2$@MgAl core-shell system as a tool to prepare well-oriented and highly active catalysts

Tomasz Kondratowicz [a], Stanislav Slang [b], Lada Dubnová [a], Oleg Kikhtyanin [c], Petr Bělina [d], Libor Čapek [a,*]

[a] University of Pardubice, Faculty of Chemical Technology, Department of Physical Chemistry, Studentská 573, 532 10 Pardubice, Czech Republic
[b] University of Pardubice, Faculty of Chemical Technology, Center of Materials and Nanotechnologies, Studentská 95, 532 10 Pardubice, Czech Republic
[c] Technopark Kralupy, University of Chemistry and Technology Prague, nám. G. Karse 7/2, 278 01 Kralupy nad Vltavou, Czech Republic
[d] University of Pardubice, Faculty of Chemical Technology, Department of Inorganic Technology, Studentská 95, 532 10 Pardubice, Czech Republic

ARTICLE INFO

*Keywords:*
Core-shell structures
Layered double hydroxides
MgAl catalysts
Aldol condensation
Base catalysis

ABSTRACT

This manuscript presents the preparation of well-oriented @MgAl-layered double hydroxides (LDHs). It extends the reported preparation of $SiO_2$@MgAl-LDH core-shell material (Si/(Si + Mg + Al) molar ratio = 0.54, Mg/Al = 2). There is introduced a new method for the gradual and controlled removal of the $SiO_2$ core from $SiO_2$@MgAl-LDH on treatment with a NaOH solution (1 M) for 1, 2, 4, and 6 h Si/(Si + Mg + Al) molar ratio from 0.06 to 0.52, Mg/Al = 2). Subsequent $SiO_2$ leaching led to empty spheres with properties of the crystalline MgAl-LDH phase preserved. It is proved that @MgAl-LDH spheres formed do not collapse and hence, preserve their original spherical shape and structural properties. The potential of @MgAl-mixed oxides (MOs) obtained by thermal treatment of @MgAl-LDHs in catalysis is also demonstrated. When this material was used for the aldol condensation reaction of furfural with acetone, the best furfural conversion was obtained for @MgAl-MO with a Si/(Si + Mg + Al) molar ratio of 0.11.

## 1. Introduction

Layered double hydroxides (LDHs) and mixed oxides (MOs) are of considerable interest to researchers and have ever-increasing demand due to their valuable qualities. These materials possess features such as acid-base properties, memory effect, anion and cation-exchange ability, and adsorption capacity (Nishimura et al., 2013; Qu et al., 2016). LDHs and MOs under different combinations of metal ions, $M(^{II})$ and $M(^{III})$ [$M(^{II})$: Mg, Zn, Ni, Cu, Co, and $M(^{III})$: Al, Fe, Ga, Cr, and Mn], are attractive candidates in many organic reactions requiring basic catalysts. For example, reactions such as aldol condensation (Bing et al., 2018; Hora et al., 2014), Knoevenagel condensation (Shirotori et al., 2014), Cannizzaro reaction (Kikhtyanin et al., 2016), epoxidation (Hoyos-Castaño et al., 2019) and transesterification (Zeng et al., 2014).

Recently, processes such as delamination and exfoliation of LDH nanosheets (Wang and O'Hare, 2012; Yu et al., 2017), aqueous miscible organic solvent treatment (AMOST) method (Chen et al., 2020; Chen et al., 2014) and immobilisation of LDHs on supports (Chen et al., 2013b; Shao et al., 2012a) have been proposed to upgrade the textural properties as well as irregular shape and size of LDHs. These processes also improve the diffusion limitations and accessibility of the active sites. Several efforts have been devoted to the synthesis of core-shell composites with well-defined morphologies and tuneable functions (Boccalon et al., 2020; Gu et al., 2015). Over the last decade, various core-shell LDH-based systems have been reported, with the core of $SiO_2$ (Chen et al., 2015; Suo et al., 2019; Suo et al., 2018), $Fe_xO_y$ (Li et al., 2019; Mi et al., 2011; Pan et al., 2011), $TiO_2$ (Dou et al., 2015), $Cu_2O$ (Wang et al., 2017), SiC (Lee and Lee, 2020), ZnO (Clark et al., 2020), zeolite (Li et al., 2018; Lyu et al., 2020; Wang et al., 2021), MOF (Lyu et al., 2020), carbon (Ni et al., 2017) and Al metal particles (Kim and Lee, 2016).

Such materials are commonly synthesised by coprecipitation, sol-gel

; 1,4-pentadien-3-one, 1,5-di-2-furanyl, $F_2Ac$; 4-(2-furyl)-3-buten-2-one, FAc; 4-(2-furyl)-4-hydroxy-butan-2-one, FAc-OH; acetone, Ac; aqueous miscible organic solvent treatment, AMOST; furfural, F; layered double hydroxides, LDHs; mesopore volume, $V_{meso}$; micropore volume, $V_{micro}$; mixed oxides, MOs; specific surface area determined by the BET method, $S_{BET}$; temperature-programmed analysis, TPA; temperature-programmed desorption of carbon dioxide, TPD-$CO_2$; total pore volume, $V_{total}$.

* Corresponding author.
*E-mail address:* libor.capek@upce.cz (L. Čapek).

https://doi.org/10.1016/j.clay.2021.106365
Received 22 August 2021; Received in revised form 19 November 2021; Accepted 23 November 2021
Available online 3 December 2021

method, and direct deposition (Gu et al., 2015). The selection of an appropriate strategy for LDH immobilisation is crucial for the orientation of platelets onto the support (Wang et al., 2020). Wang et al. (Wang et al., 2020) synthesised vertically and horizontally oriented $SiO_2$@MgAl-LDHs by sol-gel and self-assembly processes, whereas $SiO_2$@MgAl-LDH with mixed platelet morphology was obtained via a coprecipitation technique. Chen et al. (Chen et al., 2012; Zhang et al., 2013) reported $Fe_3O_4$@LDH structures with a different morphologies resulting from solvents containing different ratios of methanol to water. Generally, LDH sheets and inorganic cores interact via electrostatic forces and $M_1$-O-$M_2$ ($M_1$ and $M_2$ are metal ions) covalent bonds (Gu et al., 2015). Thus, the formation of different shell-morphologies can be explained by the nucleation speed and crystal growth mode in various synthesis pathways. For example, the formation of the vertically oriented LDH in $Fe_3O_4$@CuNiAl-LDH was attributed to the violent nucleation of LDH compactly packed on the support. Because of the limited growth space on the core surface, the LDH crystal growth on the (110) plane was faster than that on the (003) plane (Gu et al., 2015; Chen et al., 2012).

The well-oriented $SiO_2$@LDH hybrids are very common and widely studied in the literature, mainly due to: (i) relatively uncomplicated and fast synthesis of spherical $SiO_2$ core via the Stöber process (Stöber, 1968), (ii) easy and tuneable control of the $SiO_2$ particle size, and (iii) high stability of $SiO_2$@LDH involving Si-O-M covalent bonds (Chen et al., 2012). The vertically oriented platelets created an open honeycomb-like LDH shell that could be prepared by a simple ultrasound-assisted method (Chen et al., 2013a). Chen et al. (Chen et al., 2013a) fabricated a well-dispersed $SiO_2$@MgAl-LDH nanocomposite consisting of $SiO_2$ spheres with diameters of 500 nm and MgAl-LDH coatings with the thicknesses of approximately 70–100 nm. The authors stressed that two major factors were responsible for the successful formation of a well-oriented core-shell system: (i) removal of free electrolytes after precipitation and (ii) ultrasound treatment during the growth and ageing of LDH nanosheets. Kwok et al. (Kwok et al., 2018) reported that greater coverage and thicker LDH shells that were dominantly perpendicular to the $SiO_2$ surface could be obtained at a slow metal addition rate and a moderate stirring speed (500 rpm). Suo et al. (Suo et al., 2018) studied the effect of the AMOST method using acetone on the properties of a series of dendritic $SiO_2$@MgAl-LDH composites with molar ratios of 2, 3, and 4 with respect to Mg/Al in the shell. The thickness of the LDH coating in the parent materials increased from 110 to 269 nm with an increasing Mg/Al molar ratio. However, after applying the AMOST method, the thickness decreased and it ranged from 92 to 162 nm. Nevertheless, specific surface area and total pore volume increased after dispersion in organic solvents (20*h*) 52 $m^2 \cdot g^{-1}$ and 0.35 $cm^3 \cdot g^{-1}$ to 144 $m^2 \cdot g^{-1}$ and 0.60 $cm^3 \cdot g^{-1}$, respectively.

In the above-mentioned classical core-shell system, different spherical morphologies can be obtained, owing to the possibility of partial dissolution of the $SiO_2$ template in alkaline (e.g. NaOH) or acidic (e.g. HF) media (Arnal et al., 2006). The pH and temperature used during the synthesis of $SiO_2$@MgAl-LDH affected its morphology (Chen et al., 2015). Under the standard approach (pH = 10, room temperature), classical core-shell particles were produced. However, as the temperature increased to 40 °C, a yolk-shell structure was created, and at pH = 11 (at 40 °C), a deeper dissolution of the $SiO_2$ core occurred leading to a hollow shell. Under these conditions, the resulting systems possessed surface areas of 107, 118, and 177 $m^2 \cdot g^{-1}$, respectively. Shao (Shao et al., 2012b) and Zhang et al. (Zhang et al., 2016) also reported a similar observations. The authors obtained a tuneable architecture, from core-shell to hollow spheres, utilising an in situ growth technique employing spherical $SiO_2$ grains as a sacrificial template.

Different types of $SiO_2$@MgAl hybrids served as promising adsorbents for water purification (Chen et al., 2013a), electrocatalysts for the water oxidation reaction (Zhang et al., 2016), a catalyst for the hydroxylation of phenol (Zhang et al., 2013), synthesis of propylene glycol methyl ester (Wang et al., 2020), and catalytic supports to ensure a high degree of dispersion of the catalytically active phase (Mi et al., 2011).

However, to date, only two reports have described the utilisation of these materials in base catalysis, more specifically in condensation reactions (Shirotori et al., 2017, 2018). Shirotori et al. (Shirotori et al., 2017) studied the catalytic effect of various types of $SiO_2$@LDH in the Knoevenagel condensation reaction of benzaldehyde with ethyl cyanoacetate. The study included $SiO_2$@LDH system assembled with two different dimensions of $SiO_2$ spheres (40 and 250 nm) and shell composition ($M^{(II)}$: Mg, Ni, and $M^{(III)}$: Al, Ga, and $M^{(II)}/M^{(III)}$: 1 or 3). The coexistence of two different dimensions and compositions of spherical $SiO_2$ did not affect the structure of the LDH unit; however, the $SiO_2$ core plays a key role as a promoter in increasing the number of hydroxide layers acting as surface base sites, which contributes to strengthening the catalytic efficiency. Moreover, the authors suggested that the higher catalytic activity of $SiO_2$@LDHs compared to reference materials (commercial LDH and LDH obtained by the classical coprecipitation technique with and without urea) is affected not only by 3D hierarchical nanoarchitectures, but also by the fine LDH crystallite size. Among the $SiO_2$@MgAl nanocomposites with different atomic ratios of Si/(Mg + Al), the highest reaction rate of 171 $mmol \cdot g^{-1} \cdot h^{-1}$ was observed in the Knoevenagel condensation for Si/(Mg + Al) = 0.17. It is worth emphasising that this value is 2.2 times higher than the classical LDH prepared without the $SiO_2$ core (Shirotori et al., 2018).

This manuscript present a method to improve the morphology, textural properties, and accessibility of the active sites of LDHs and MOs. $SiO_2$@MgAl-LDH core-shell was employed as the starting material to establish the method. There is introduced a process, based on the gradual and controlled removal of the $SiO_2$ core from $SiO_2$@MgAl-LDH, leading to well-oriented @MgAl-LDH materials. The schematic of the post-synthesis treatment is shown in Fig. 1. The effects of the gradual removal of the $SiO_2$ core on the structural, textural, and basic properties of the core-shell material are described here. The potential of such materials in catalysis (aldol condensation of furfural with acetone) has also been demonstrated.

## 2. Experimental

### 2.1. Synthesis

Monodisperse $SiO_2$ microspheres were synthesised by the modified Stöber process (Stöber, 1968). Briefly, an amount of 128 g of ethanol (Lach-Ner, 96%) together with 54 mL of an aqueous solution of $NH_3$ (Lach-Ner, 25%) was introduced into a round bottom flask (500 mL). After heating to 30 °C, 8.4 mL of TEOS (Sigma-Aldrich, 98%) was quickly added and the mixture was left under stirring for 1 h. The fabricated spherical $SiO_2$ particles were centrifuged (4900 rpm, 10 min) and washed five times in water (100 mL). Each time, the particles were dispersed in an ultrasonic bath (for 10 min) and again isolated by centrifugation. Finally, the solid sample was dried at 60 °C overnight.

The spherical core-shell $SiO_2$@MgAl-LDH composite was prepared by coprecipitation of Mg and Al precursor in the presence of hard template - non-porous spherical $SiO_2$ particles with uniform in size with the diameters ca. 500 nm, according to the protocol (Kwok et al., 2018; Shirotori et al., 2017) with some modifications. In details, 100 mg of spherical $SiO_2$ particles were dispersed in 20.0 mL of deionized water using ultrasound treatment (1 h). Subsequently, 0.96 mmol of $Na_2CO_3$ (Lach-Ner, 100.1%) was added to the milky solution and dispersed for another 10 min. To so prepared suspension added dropwise 19.2 mL water solution containing 0.96 mmol $Mg(NO_3)_2 \cdot 6H_2O$ (Lach-Ner, 100.8%) and 0.48 mmol $Al(NO_3)_3 \cdot 9H_2O$ (Lach-Ner, 98.6%) (addition rate 1 mL/min, stirring speeds of 400 rpm). The pH was maintained at 10.00 ± 0.03 using an aqueous NaOH solution (1 M) during titration. After 2 h of stirring, the obtained core-shell composite was filtered, washed with 2 L of water and dried at 60 °C overnight. Sample after dried denoted as $SiO_2$@MgAl-LDH.

In the next step, the $SiO_2$ core was etched under static conditions by treatment with a NaOH solution (1 M) at 30 °C for 1, 2, 4, and 6 h. To

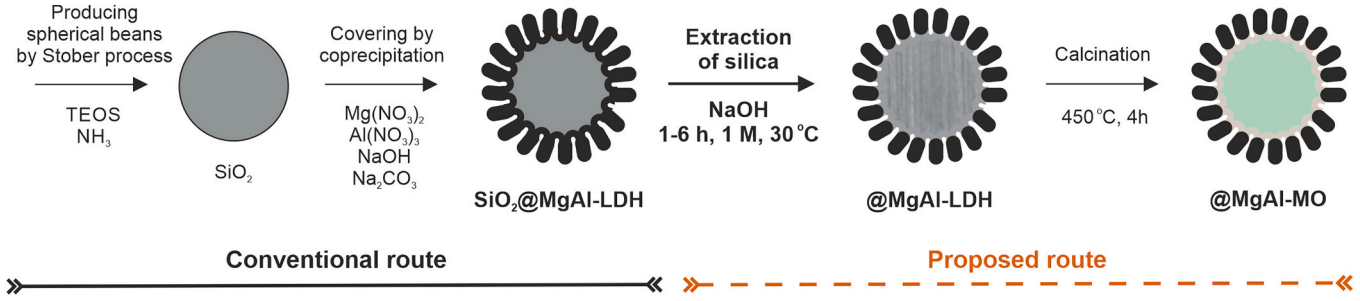


**Fig. 1.** Synthesis pathway used to obtain @MgAl-MO catalysts.

remove remaining $Na^+$, the obtained particles were thoroughly washed with distilled water and then dried at 60 °C. The obtained materials denoted as @MgAl-LDH_*x*h, where *x* expresses the etching time.

$SiO_2$@MgAl-LDH_ChM (material with chaotic morphology) was synthesised as follows. 100 mg of silica spheres were dispersed in 20 mL of deionized water by ultrasound treatment for 1 h, followed by adding 0.8 mL of aqueous ammonia solution. Then 19.2 mL of an aqueous solution containing 0.96 mmol $Mg(NO_3)_2{\cdot}6H_2O$ and 0.48 mmol $Al(NO_3)_3{\cdot}9H_2O$ was dropped (1 mL/min) under vigorous stirring, without pH control. After 1 h of stirring, the solid particles were obtained by centrifugation.

MgAl-based mixed oxides were obtained by thermal treatment of LDH-like precursor in air at 450 °C for 4 h (heating rate of 5 °C/min) in a muffle oven. Calcined samples are denoted as $SiO_2$@MgAl-MO, $SiO_2$@MgAl-MO_ChM and @MgAl-MO_*x*h, respectively.

### 2.2. Characterization

The quantitative EDX measurements were performed on electron microscope (LYRA3, Tescan) equipped with EDX analyzer AZtec X-Max 20 (Oxford Instruments) at an acceleration voltage of 20 kV (an accelerating voltage possessing a signal from a depth of micrometres, which is sufficient for the studied core-shell particles with dimensions of approximately 750 nm). The samples were covered with 20 nm of carbon by Leica EM ACE200 coater, measured on 5 different spots with a size of 200 μm × 200 μm, which is higher than the size of the studied particles and obtained compositions were averaged. A scanning electron microscope (LYRA3, Tescan) was used for surface morphology study using 10 kV acceleration voltage. Transmission electron microscopy (TEM) measurements were carried out on a FEI Tecnai TF20 X-TWIN (FEG) microscope equipped with an energy-dispersive X-ray spectrometer (EDAX), working at an accelerating voltage of 200 kV. Samples for the TEM observations were prepared by *drop-casting* on *carbon-coated* copper grids. The crystallographic structure of samples was determined by Bruker AXS D8-Advance diffractometer using Cu Kα radiation (λ = 0.154 nm) with a secondary graphite monochromator. The XRD patterns were recorded in range of 2θ = 5–80° with a step of 0.02°. Nitrogen adsorption-desorption isotherms were measured by using a Micromeritics TriStar II instrument. Samples were degassed for 6 h under vacuum at 130 °C or 150 °C for LDH and MO phase, respectively. Specific surface areas were determined by the BET method ($S_{BET}$). Total pore volumes ($V_{total}$) were obtained from amounts of nitrogen adsorbed at relative pressure of 0.99, whereas micropore ($V_{micro}$) and mesopore ($V_{meso}$) volumes were calculated using the t-plot and Barrett-Joyner-Halenda (BJH) models, respectively. Temperature-programmed desorption of carbon dioxide (TPD-$CO_2$) was performed using a Micromeritics AutoChem II 2920 equipped with a TCD detector and OmniStar quadrupole mass spectrometer. 100 mg of a sample was outgassed in a flow of helium (20 mL/min) at 450 °C for 1 h, and then cooled down to 25 °C. The $CO_2$ uptake from a stream of 10 vol% of $CO_2$ in He (a flow rate of 20 mL/min) for 30 min. Weakly adsorbed $CO_2$ was removed by flushing with He at 25 °C for 1 h. The desorption of $CO_2$ was analyzed (the molecular ion, $m/z = 44$) in the temperature range of 25–450 °C at the heating rate of 10 °C/min.

### 2.3. Catalytic tests

Aldol condensation of the stabilized furfural with acetone (99.98%, Penta, Czech Republic) was carried out in a 100 mL stirred batch reactor (a glass flask reactor) at the temperature of 50 °C at ambient pressure. Acetone (37.90 g) to furfural (6.27 g) molar ratio was 10:1. Furfural (99%, Sigma-Aldrich) was distilled using a vacuum rotary-evaporator and then stabilized with 2,6-di-tert-butyl-4-methylphenol (DBMP, 99%, Sigma-Aldrich) using weight ratio DBMP/Furfural = 0.04). Acid impurities in furfural were neutralized. Prior to the catalytic tests, 1.00 g of a sample with particle size in the range of 250–500 μm (freshly calcined in a muffle oven at 450 °C and stored in a desiccator) was added, and the reaction was carried out for 240 min at 400 rpm. For details and the formula for calculating the conversion and selectivity values see (Kikhtyanin et al., 2021).

## 3. Results and discussion

### 3.1. Features of spherical $SiO_2$@MgAl-LDH and @MgAl-LDHs

Table 1 lists the Mg/Al and Si/(Si + Mg + Al) molar ratios of $SiO_2$@MgAl-LDH and @MgAl-LDHs ($SiO_2$@MgAl-LDH after the leaching of the $SiO_2$ core for periods of 1, 2, 4, and 6 h). Based on SEM-EDX, the initial $SiO_2$@MgAl-LDH contained a Si/(Si + Mg + Al) molar ratio of 0.54. The treatment of $SiO_2$@MgAl-LDH in an alkaline medium for a period of 1 and 2 h caused a slight decrease in this ratio to 0.52 and 0.47, respectively. It was noted that ICP studies and SEM-EDX analysis agree with each other. Subsequently, a much higher elimination of the $SiO_2$ core was observed after 4 and 6 h, when the Si/(Si + Mg + Al) molar ratio dropped to 0.11 and 0.06, respectively. It should be stressed that the Mg/Al molar ratio was approximately the same for all materials studied (Mg/Al = approximately 2) (Table 1).

To determine the maximum possible amount of $SiO_2$ core that could be removed, more severe conditions for leaching were employed. Higher leaching times of 24 and 48 h were used (while maintaining the temperature and concentration of NaOH solution) and much stronger leaching conditions (2 M, 50 °C, and 20 h) were studied. In all these cases, the Si/(Si + Mg + Al) molar ratio was in the range 0.05–0.06. Thus, complete extraction of $SiO_2$ from $SiO_2$@MgAl-LDH was not possible. The formation of Si-O-Al and Si-O-Mg covalent bonds between Mg Al platelets and the $SiO_2$ core was responsible for the incomplete extraction of $SiO_2$ (Chen et al., 2015; Kwok et al., 2018; Shirotori et al., 2017, 2018; Suo et al., 2018). The residual amount of $SiO_2$ has also been reported in core-shell systems containing the $SiO_2$ core and NiAl-LDH (Shao et al., 2012b), $TiO_2$ (Güttel et al., 2011), and $ZrO_2$ (Kondratowicz et al., 2019) shells.

Fig. 2 shows XRD patterns of $SiO_2$@MgAl-LDH and @MgAl-LDHs. The patterns of all materials contained diffraction lines at 11.5°, 23.2°, 34.8°, 39.3°, 46.7°, 60.8°, and 62.1°, which could be assigned to the (0

**Table 1**
Chemical composition and crystal properties of the $SiO_2$@MgAl-LDH composites before and after leaching.

| Sample | Molar ratios | | Lattice parameter [nm] | | LDH basal spacing [nm] | Crystallite Size [nm] | |
|---|---|---|---|---|---|---|---|
| | Mg/Al | Si/(Si + Mg + Al) | a | c | d | D(003) | D(110) |
| $SiO_2$@MgAl-LDH | 2.00[a]<br>1.91[b] | 0.54[a]<br>0.57[b] | 0.3047 | 2.3044 | 0.768 | 7.4 | 12.3 |
| @MgAl-LDH_1h | 2.08[a]<br>2.03[b] | 0.52[a]<br>0.56[b] | 0.3046 | 2.3060 | 0.769 | 7.6 | 13.3 |
| @MgAl-LDH_2h | 2.05[a]<br>2.00[b] | 0.47[a]<br>0.51[b] | 0.3048 | 2.3044 | 0.768 | 7.6 | 13.3 |
| @MgAl-LDH_4h | 1.98[a] | 0.11[a] | 0.3051 | 2.3048 | 0.768 | 7.3 | 13.1 |
| @MgAl-LDH_6h | 2.01[a] | 0.06[a] | 0.3051 | 2.3069 | 0.769 | 7.7 | 13.5 |

[a] SEM-EDX.
[b] ICP

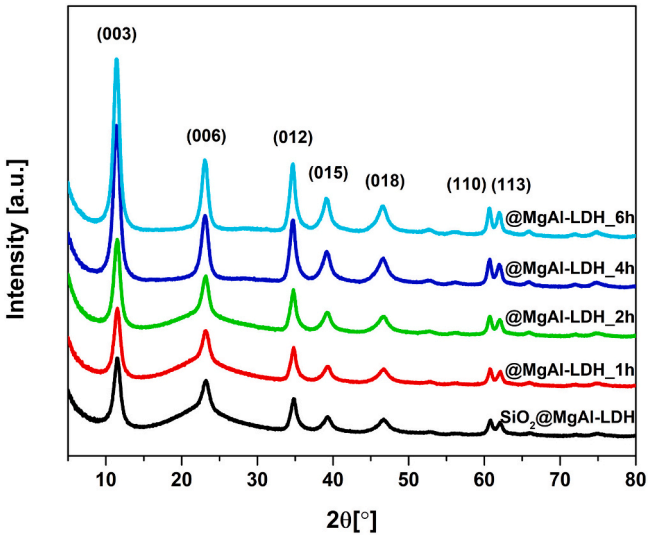


**Fig. 2.** XRD patterns of the $SiO_2$@MgAl-LDH composite before and after the $SiO_2$ core etching with 1 M NaOH solution at various time periods.

0 3), (0 0 6), (012), (0 1 5), (0 1 8), (1 1 0), and (113) planes typical of the MgAl double-layered structure in the trigonal R-3 m space group (PDF Card No. 01–070-2151). The broad hump at $2\theta = 22°$, which is attributed to the presence of amorphous $SiO_2$ in the $SiO_2$@MgAl-LDH composite, became less intense with increasing $SiO_2$ leaching time and finally disappeared after 4 h. First, the positions of the above-mentioned diffraction lines did not change after the leaching of the $SiO_2$ core. Second, the unit cell parameters $a$ ($a = 2d_{110}$) and $c$ ($c = 3d_{003}$), as well as LDH basal spacing (interlayer distance along the $c$-axis, $d$-value) are almost identical for $SiO_2$@MgAl-LDH and @MgAl-LDHs, regardless of the time of $SiO_2$ leaching (Table 1). The unit cell in the crystal lattice corresponds to the data reported for conventional pure and bulk MgAl-LDHs with a similar Mg/Al molar ratios (Creasey et al., 2014; Kikhtyanin et al., 2017). Third, the crystallite size of LDH for the stacking direction D(0 0 3) and plane direction D(1 1 0) present in $SiO_2$@MgAl-LDH are equal to 7.4 and 12.3 nm, respectively. After treatment in an alkaline environment, these values remained almost unchanged in @MgAl-LDHs, and the values were in the ranges 7.3–7.7 and 13.1–13.5 nm, respectively (Table 1).

Although the partial loss of LDH could not be excluded during the process of $SiO_2$ leaching, the results mentioned above clearly show the presence of the crystalline MgAl-LDH phase in @MgAl-LDHs with the same properties as in the initial $SiO_2$@MgAl-LDH.

Higher values of crystallite size for the plane direction than stacking direction have also been reported by Shirotori et al. (Shirotori et al., 2017, 2018) for core-shell materials constructed with $SiO_2$ cores and NiAl, MgGa, and MgAl-LDH shell. The authors attributed this observation to the coexistence of spherical $SiO_2$ particles during the gradual addition of the LDH precursor, which resulted in good dispersion of the starting points of LDH crystal growth on the $SiO_2$ surface. Moreover, a rapid nucleation of LDH on the surface of the support, and simultaneously a faster growth of the LDH crystal on the (1 1 0) plane than on the (0 0 3) plane, assists the formation of core-shell systems wherein the LDH plates are oriented perpendicular to the surface of the support (Gu et al., 2015; Chen et al., 2012). Based on the above explanation, vertical immobilisation of MgAl platelets onto $SiO_2$ spheres is suggested for $SiO_2$@MgAl-LDH.

SEM (Fig. 3A) and TEM images (Fig. 4A) show the spherical shape of the prepared $SiO_2$@MgAl-LDH. A well-defined core-shell structure is visible, built by a $SiO_2$ core with a diameter of ~500 nm and a shell with an average thickness of ~120 nm (TEM). Moreover, the outer layer of the composite consisted of perpendicularly oriented MgAl-LDH platelets on the $SiO_2$ surface. No considerable changes were observed in the shape and size of the spheres formed after partial leaching of the $SiO_2$ core from $SiO_2$@MgAl-LDH for 1 h (@MgAl-LDH_1h) and 2 h (@MgAl-LDH_2h) (Fig. 3B and C). This is related to the low degree of $SiO_2$ removal Si/(Si + Mg + Al) molar ratio, which decreased for these materials from 0.54 to 0.52 and 0.47.

In contrast, a significant change in morphology was observed in @MgAl-LDH materials obtained after treatment for periods of 4 and 6 h. This change in morphology is also associated with a significant decrease in the Si/(Si + Mg + Al) molar ratio (up to 0.11 and 0.06, respectively) (Fig. 3D and E). Some of the spheres were partially cracked with a well-visible hollow space inside the grains. The size of the void agrees perfectly with the diameter of the washed $SiO_2$ matrix. It is important to emphasise that the formed empty spheres do not collapse in @MgAl-LDHs, preserving their original spherical shape originating from the $SiO_2$ core. Moreover, after deep removal of the silica, the contrast between the core and shell disappeared (Fig. 4B), which confirms the removal of the template. Generally, the fabricated LDH sphere possesses a hollow space inside, which exists despite the lack of a cracked surface of the sphere. However, in some cases, a visible hole in the sphere was observed owing to the cracked surface. There are two explanations for this finding:

(i) This could reflect the partial removal of LDH from core-shell materials. However, the crystalline LDH phase had the same properties before and after $SiO_2$ leaching (XRD results). It therefore raises a question: if the crystalline LDH phase was removed, why had it occurred only in one sphere? Furthermore, the lack of additional mass losses determined after the etching operation indicated that the MgAl phase was stable during the dissolution of $SiO_2$. Thus, the dissolution of the LDH phase was not probable during the leaching of $SiO_2$ from $SiO_2$@MgAl-LDH.
(ii) It should be noted that the spherical $SiO_2$ particles after ultrasonic treatment may also have aggregated. Thus, the MgAl-LDH precursor could not be deposited on the contact surface. In such a case, a more complex system exists after $SiO_2$ removal, which can

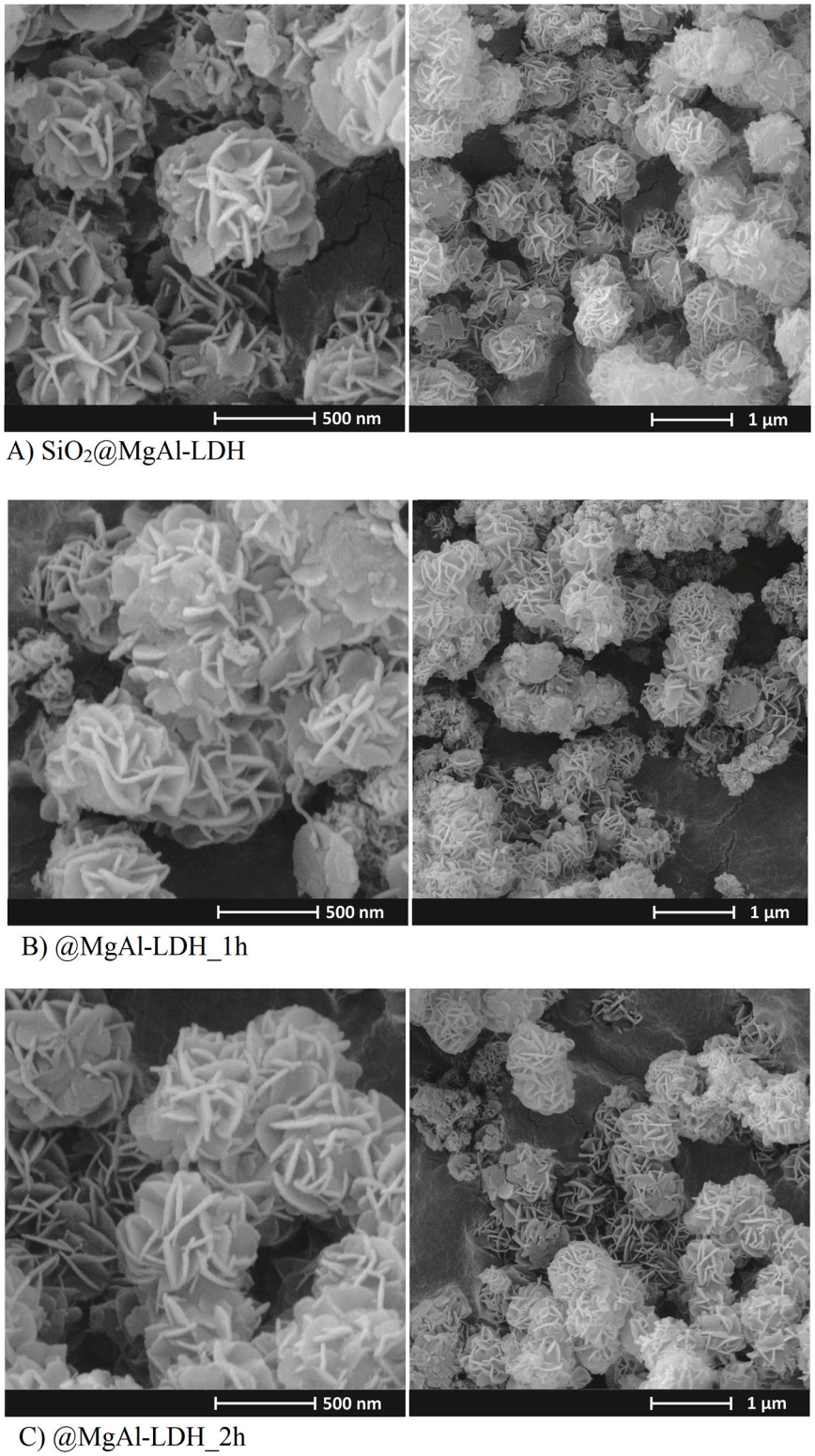


**Fig. 3.** SEM images of $SiO_2$@MgAl-LDH (A) and @MgAl-LDH etched with 1 M NaOH at 30 °C for 1 (B), 2 (C), 4 (D) and 6 (E) hours.

rupture, resulting in visibly hollow spheres. This was a more probable reason.

The $N_2$ adsorption isotherms of $SiO_2$@MgAl-LDH and @MgAl-LDHs are shown in Fig. 5. The textural parameters are listed in Table 2. The starting $SiO_2$@MgAl-LDH had a BET surface area of 65 $m^2 \cdot g^{-1}$ and a total pore volume of 0.30 $cm^3 \cdot g^{-1}$. The $N_2$ adsorption isotherm for this material is the closest to the IVa type according to the IUPAC classification, which is typical of *meso*porous materials containing pores wider than ~4 nm (Thommes et al., 2015). Moreover, a type H3 loop is present, which is characteristic of non-rigid aggregates of plate-like particles (Thommes et al., 2015).

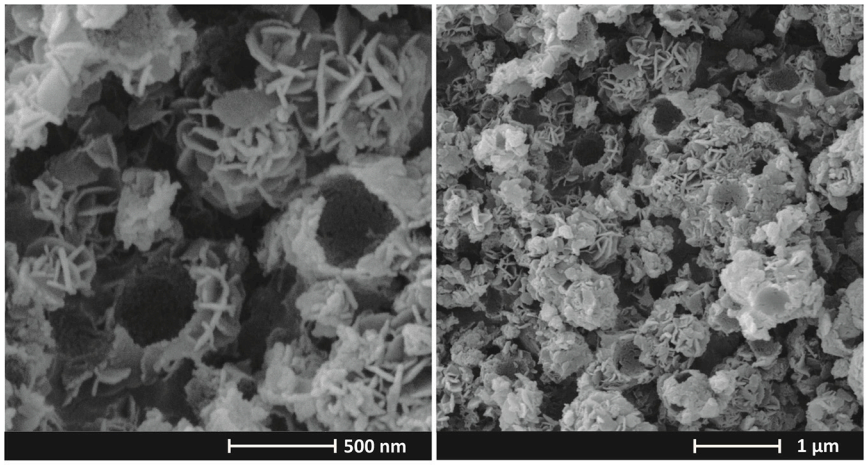


D) @MgAl-LDH_4h

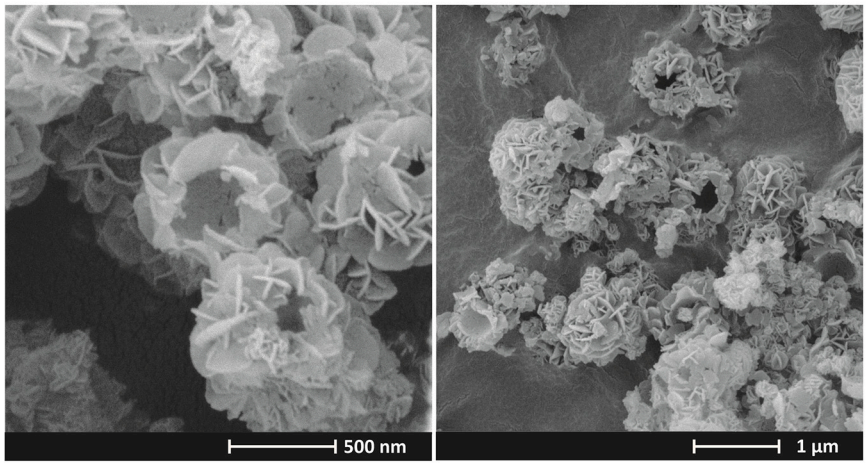


E) @MgAl-LDH_6h

**Fig. 3.** (*continued*).

The gradual elimination of $SiO_2$ from $SiO_2$@MgAl-LDH resulted in an increased total pore volume originating from the increase in the volume of meso and macropores (Table 2). The progressive leaching of the $SiO_2$ core led to a gradual increase of the volume of mesopores and macropores up to 0.39 $cm^3 \cdot g^{-1}$ and 0.24 $cm^3 \cdot g^{-1}$, respectively. The pore volume of original $SiO_2$@MgAl-LDH, @MgAl-LDH_1h and @MgAl-LDH_2h materials range from 0.13 to 0.17$cm^3 \cdot g^{-1}$. Thus, it could be suggested that macropores are mainly formed in these materials by spaces located between spherical grains (the interparticle porosity). However, for both @MgAl-LDH_4h and @MgAl-LDH_6h materials, this value increased to 0.24 $cm^3 \cdot g^{-1}$. This significant growth could be explained by the appearance of empty spaces inside the formed grains, which is also visible in the SEM (Fig. 3D and E) and TEM images (Fig. 4B). The effect of removing the $SiO_2$ core is also manifested in the BET surface area changes, which initially increased to 210 and 293 $m^2 \cdot g^{-1}$ after periods of 1 and 2 h of alkali treatment, respectively. This was attributed to the partial destruction of $SiO_2$. It then decreased to 197 $m^2 \cdot g^{-1}$ and 165 $m^2 \cdot g^{-1}$ after a treatment period of 4 and 6 h for $SiO_2$ core removal, respectively, owing to the formation of hollow spheres.

### 3.2. Spherical $SiO_2$@MgAl-MO and @MgAl-MO catalysts

The XRD patterns of $SiO_2$@MgAl-MO and @MgAl-MOs (Fig. 6) show a broad signal at 22°, characteristic of amorphous $SiO_2$. In addition, three diffraction lines at ~35.1°, 43.1°, and 62.5° were observed, which can be assigned to the (111), (200), and (220) planes, respectively, of the MgO-like phase (periclase) or a magnesia-alumina solid solution (PDF Card No. 00–004-0829). Thus, the aluminium species should be well dispersed in the MgO phase without the formation of segregated phases or an amorphous phase (Čapek et al., 2013; Hora et al., 2015; León et al., 2010). It should be noted that the intensities of these reflections grew slightly with an increase in etching time because of the decrease in the Si/(Si + Mg + Al) molar ratio. However, reflections corresponding to the $MgAl_2O_4$ spinel phase were not detected, which was in line with the literature, which states that the formation of this phase occurs at much higher temperatures (approximately 800–1000 °C) (Čapek et al., 2013; Ganesh, 2013).

The shapes of the $N_2$ adsorption isotherms for both $SiO_2$@MgAl-MO and @MgAl-MOs did not change significantly in comparison to the original LDH-based materials, whereas the textural properties for most of the systems changed significantly (Table 3).

The volume of meso and macropores and the total porosity of @MgAl-MO materials show an increasing trend, which was compatible with a gradual decrease in the Si/(Si + Mg + Al) molar ratio. Overall, considering that the total pore volume was in the range 0.34–0.86 $cm^3 \cdot g^{-1}$ and micropore volume of 0.01–0.02 $cm^3 \cdot g^{-1}$, it can be concluded that the content of the latter has a negligible impact on the total porosity of the studied materials. Mainly mesopores ($V_{meso}$ = 0.18–0.46 $cm^3 \cdot g^{-1}$) play a dominant role in the pore systems of $SiO_2$@MgAl-MO and @MgAl-MOs, which are complemented by macroporous voids ($V_{macro}$ = 0.15–0.39 $cm^3 \cdot g^{-1}$).

In the literature, thermal treatment of LDHs into appropriate MOs

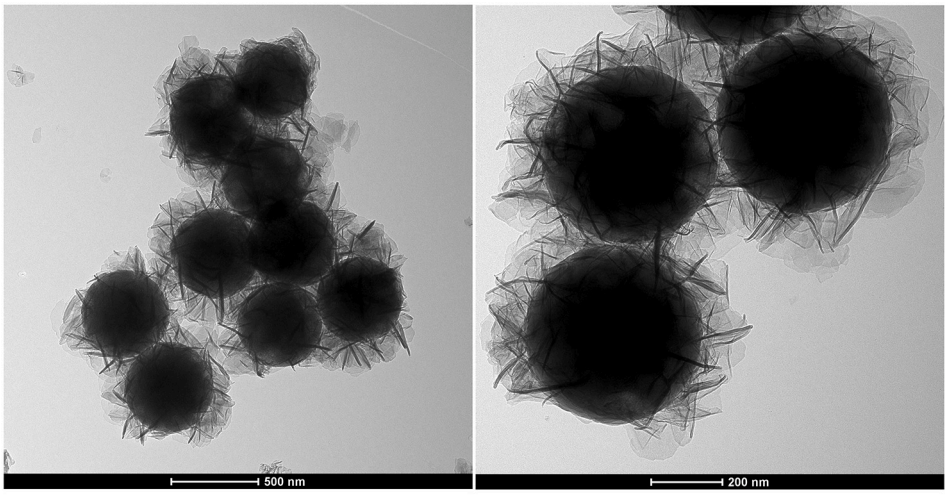


**Fig. 4.** TEM images of $SiO_2$@MgAl-LDH (A) and @MgAl-LDH etched with 1 M NaOH at 30 °C for 4 h (B).

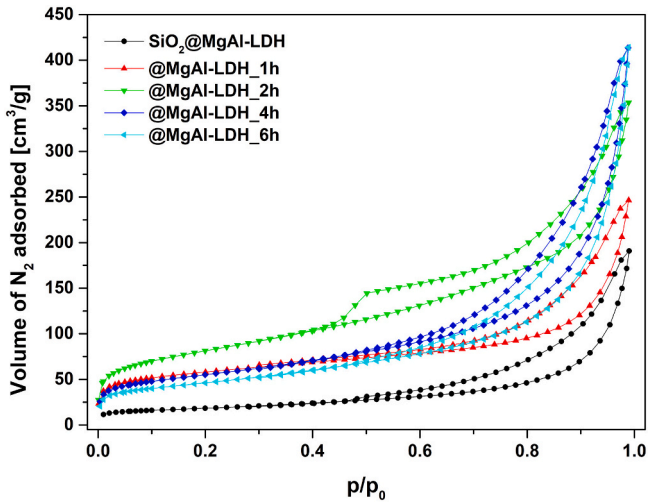


**Fig. 5.** $N_2$ adsorption isotherms of the $SiO_2$@MgAl-LDH composite before and after the $SiO_2$ core etching under different conditions.

**Table 2**
Textural properties of the $SiO_2$@MgAl-LDH and @MgAl-LDH composites.

| Sample | $S_{BET}$ [$m^2 \cdot g^{-1}$] | $V_{micro}$ [$cm^3 \cdot g^{-1}$] | $V_{meso}$ [$cm^3 \cdot g^{-1}$] | $V_{macro}$ [$cm^3 \cdot g^{-1}$] | $V_{total}$ [$cm^3 \cdot g^{-1}$] |
|---|---|---|---|---|---|
| $SiO_2$@MgAl-LDH | 65 | 0.005 | 0.156 | 0.134 | 0.295 |
| @MgAl-LDH_1h | 210 | 0.029 | 0.185 | 0.167 | 0.381 |
| @MgAl-LDH_2h | 293 | 0.015 | 0.363 | 0.169 | 0.547 |
| @MgAl-LDH_4h | 197 | 0.013 | 0.390 | 0.236 | 0.639 |
| @MgAl-LDH_6h | 165 | 0.009 | 0.395 | 0.236 | 0.640 |
| $SiO_2$@MgAl-LDH_ChM | 111 | 0.010 | 0.213 | 0.110 | 0.333 |

mainly causes expansion of the specific surface area and porosity of the formed materials (Di Cosimo et al., 1998; Hora et al., 2014). However, in our case, the trend was more complex and depended not only on the transformation of LDHs to MOs, but also on the content of the $SiO_2$ core.

Fig. 7 shows the TPD-$CO_2$ profiles of the $SiO_2$@MgAl-MO and @MgAl-MOs. For $SiO_2$@MgAl-MO, two fundamental peaks of $CO_2$ desorption with a maximum at 100 °C (low-temperature peak) and

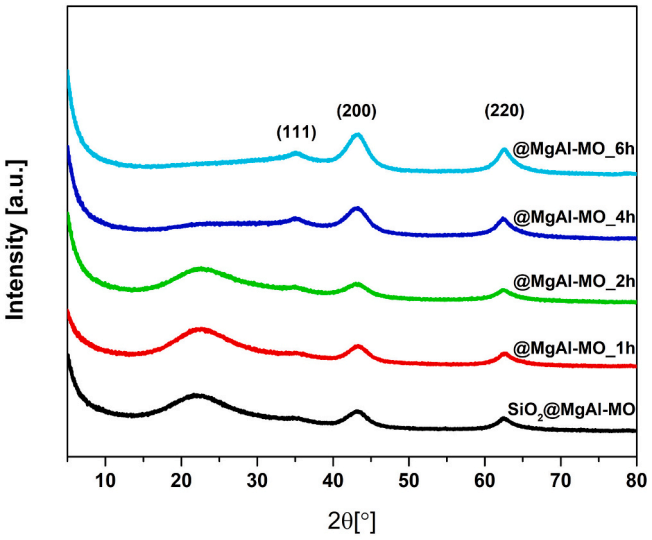


**Fig. 6.** XRD patterns of the $SiO_2$@MgAl-MO and @MgAl-MO systems.

**Table 3**
Textural properties of the $SiO_2$@MgAl-MO and @MgAl-MO composites.

| Sample | $S_{BET}$ [$m^2 \cdot g^{-1}$] | $V_{micro}$ [$cm^3 \cdot g^{-1}$] | $V_{meso}$ [$cm^3 \cdot g^{-1}$] | $V_{macro}$ [$cm^3 \cdot g^{-1}$] | $V_{total}$ [$cm^3 \cdot g^{-1}$] |
|---|---|---|---|---|---|
| $SiO_2$@MgAl-MO | 78 | 0.008 | 0.180 | 0.149 | 0.337 |
| @MgAl-MO_1h | 139 | 0.016 | 0.175 | 0.178 | 0.369 |
| @MgAl-MO_2h | 290 | 0.012 | 0.376 | 0.209 | 0.597 |
| @MgAl-MO_4h | 209 | 0.012 | 0.457 | 0.357 | 0.826 |
| @MgAl-MO_6h | 215 | 0.010 | 0.455 | 0.393 | 0.858 |
| $SiO_2$@MgAl-MO_ChM | 90 | 0.006 | 0.207 | 0.129 | 0.342 |

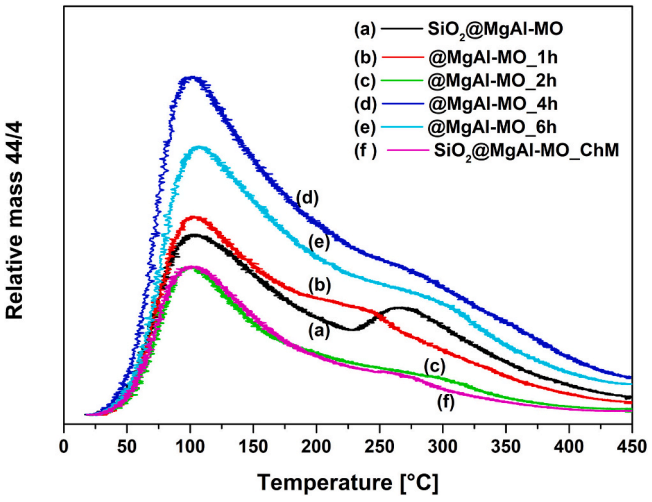


**Fig. 7.** TPD-$CO_2$ profiles of $SiO_2$@MgAl-MO and @MgAl-MO systems pre-treated at 450 °C.

270 °C (high-temperature peak) were observed. The desorption peak at 100 °C was the most intense for all the materials studied. The low-temperature peak could be attributed to the presence of weak basic sites generated by $OH^-$ groups (Bolognini et al., 2002; Di Cosimo et al., 1998; Grabowska et al., 2005; Silva et al., 2010). In the literature, the medium basic sites ($Mg^{II}$-$O^{-II}$ and $Al^{III}$-$O^{-II}$ pairs) are mainly attributed at the ranges 140–170 °C (Bolognini et al., 2002; Di Cosimo et al., 1998; Grabowska et al., 2005) and 210–220 °C (Di Cosimo, 2000; Silva et al., 2010) and the strong basic sites (isolated $O^{2-}$ ions associated with cationic vacancies) are mostly attributed to the range 270–320 °C (Di Cosimo et al., 1998; Grabowska et al., 2005; Veloso et al., 2008). Owing to a broad desorption peak, it was difficult to determine the presence of medium and strong basic sites. For all @MgAl-MOs, the clearly visible high-temperature peak vanishes and appears as a flex point on the shoulders at ~250 °C.

The total amount of basic sites was calculated as the total $CO_2$ desorbed from 25 to 450 °C (Table 4). The total number of basic sites in $SiO_2$@MgAl-MO was 108 $\mu mol \cdot g_{cat}^{-1}$. The basicity of @MgAl-MO materials is in the range 65–193 $\mu mol \cdot g_{cat}^{-1}$, but the dependence of the total concentration of basic sites on the Si/(Si + Mg + Al) molar ratio was not observed. This shows that the total concentration of basic sites [$\mu mol \cdot g_{cat}^{-1}$] was not dependent only on the relative populations of the $SiO_2$ and MgAl-MO phases, but it was a more complex case. It also depends on the contribution of the base site accessibility, the changing overall surface area of the materials, and the potential blocking of basic sites by species appearing during the $SiO_2$ removal process.

The number of basic sites was also calculated per 1 g of pure MgAl mixed oxide present in the material (Table 4). The highest number of basic sites calculated per 1 g of pure MgAl mixed oxide was found in $SiO_2$@MgAl-MO, followed by @MgAl-MO_1h with a low proportion of $SiO_2$ removal. Although @MgAl-MO_4h and @MgAl-MO_6h possessed the highest representation of MgAl mixed oxide, the significant removal of $SiO_2$ led to an increase in the basicity expressed per 1 g of catalyst [$\mu mol \cdot g_{cat}^{-1}$], but it led to lower basicity corresponding to the mixed oxide content. This indicates that the $SiO_2$ leaching process partially affects the basicity of the MgAl-MOs.

### 3.3. *Influence of morphology in the core-shell system*

To explain the role of the well-oriented morphology, $SiO_2$@MgAl-LDH_ChM material using different synthesis procedure was prepared. Both $SiO_2$@MgAl-LDH and $SiO_2$@MgAl-LDH_ChM have similar Si/(Si + Mg + Al) molar ratio (0.54 and 0.51, respectively). Nevertheless, $SiO_2$@MgAl-LDH_ChM possesses low-quality orderliness of MgAl platelets on $SiO_2$ spheres (Fig. 8). Both uncovered and partially covered $SiO_2$ matrix and areas of irregular aggregates of considerable size were visible. Hence, the term of "chaotic" morphology is considered.

Both $SiO_2$@MgAl-LDH_ChM and $SiO_2$@MgAl-LDH showed the similar shapes of $N_2$ adsorption isotherms. However, the BET surface area and total pore volume were higher for the former (111 $m^2 \cdot g^{-1}$ and 0.33 $cm^3 \cdot g^{-1}$, respectively). This could be explained by the coexistence of the core-shell system as well as pure $SiO_2$ and MgAl-LDH phases in the $SiO_2$@MgAl-LDH_ChM material. Additionally, considering the sample composition and negligible surface area of $SiO_2$ (10 $m^2 \cdot g^{-1}$), it can be stated that the pure MgAl-LDH phase possesses a higher surface area than that of the core-shell material. Subsequently, $SiO_2$@MgAl-MO_ChM also possessed higher values of $S_{BET}$ and $V_{meso}$ than $SiO_2$@MgAl-MO (90 $m^2 \cdot g^{-1}$ vs. 78 $m^2 \cdot g^{-1}$ and 0.21 $cm^3 \cdot g^{-1}$ vs. 0.18 $cm^3 \cdot g^{-1}$).

**Table 4**
Concentration of basic sites in the $SiO_2$@MgAl-MO and @MgAl-MO composites.

| Sample | Concentration of basic sites in the sample | |
|---|---|---|
| | [$\mu mol \cdot g_{cat}^{-1}$] | [$\mu mol \cdot g_{MgAl}^{-1}$] |
| $SiO_2$@MgAl-MO | 108 | 243 |
| @MgAl-MO_1h | 106 | 238 |
| @MgAl-MO_2h | 65 | 129 |
| @MgAl-MO_4h | 193 | 221 |
| @MgAl-MO_6h | 153 | 161 |
| $SiO_2$@MgAl-MO_ChM | 62 | 125 |

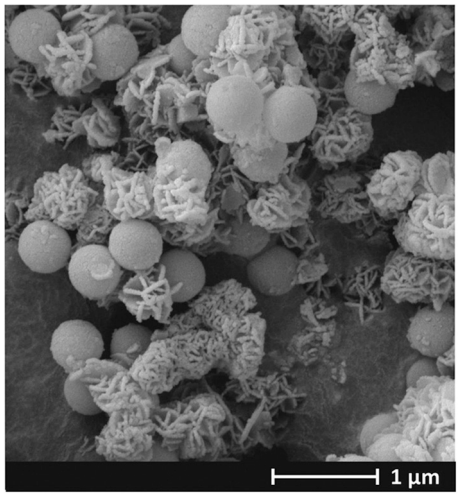


**Fig. 8.** SEM image of the $SiO_2$@MgAl-LDH_ChM.

Even with the lower specific surface area of the $SiO_2$@MgAl-MO system where the MgAl platelets are mainly vertically oriented on the $SiO_2$ matrix, the material maintained a higher total concentration of basic sites. This was almost twice the number of basic sites per gram of material and gram of MgAl phase as well (1.7 and 1.9, respectively) than $SiO_2$@MgAl-MO_ChM.

### 3.4. Catalytic performance of $SiO_2$@MgAl-MO and @MgAl-MO

Fig. 9A shows the effect of reaction time on furfural conversion under $SiO_2$@MgAl-MO and @MgAl-MOs catalysis. $SiO_2$@MgAl-MO exhibited a furfural conversion of 28% (after 4 h of reaction). A lower furfural conversion (13%) was observed for the core-shell system, which possesses a lower quality orderliness of the MgAl-MO phase ($SiO_2$@MgAl-MO_ChM).

The leaching of the $SiO_2$ core from $SiO_2$@MgAl-MO first led to a slight decrease in furfural conversion, as evidenced by the @MgAl-MO_2h catalyst (20% after 4 h of reaction). Subsequent leaching of the $SiO_2$ core led to the @MgAl-MO_4h catalyst with the highest furfural conversion values (74% after 4 h of reaction). Finally, further leaching of the $SiO_2$ core caused a decrease in furfural conversion as observed for @MgAl-MO_6h (58% after 4 h of reaction). It was important to stress that @MgAl-MO_6h catalysis offered lower furfural conversion than

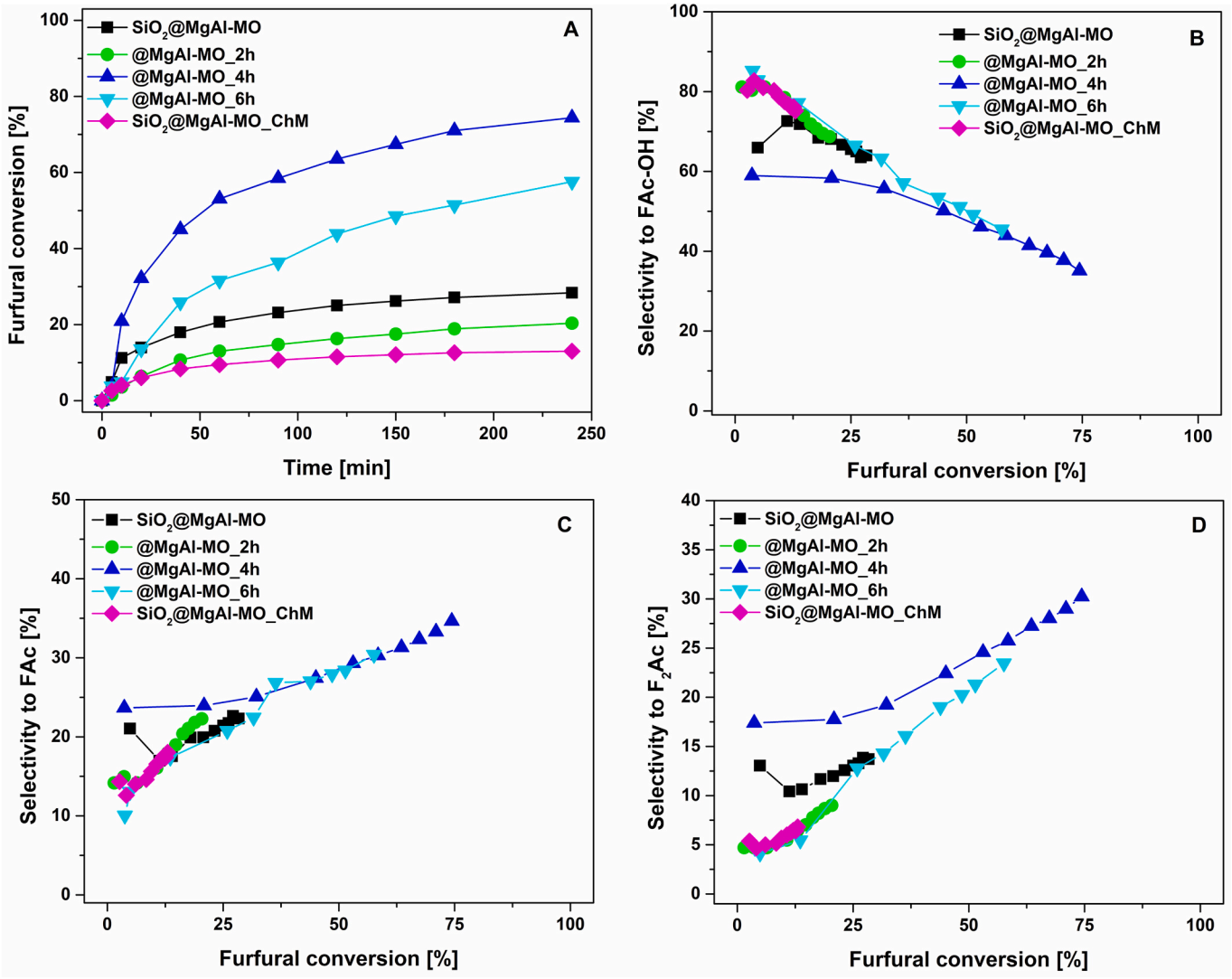


**Fig. 9.** Conversion of furfural vs. reaction time (A) and selectivity to FAc-OH (B), FAc (C) and $F_2$Ac (D) versus furfural conversion over the $SiO_2$@MgAl-MO and @MgAl-MO catalysts.

@MgAl-MO_4h, even though @MgAl-MO_6h contains a higher relative population of MgAl-MO compared to @MgAl-MO_4h. This was direct evidence that the furfural conversion was affected by the properties of the materials resulting from $SiO_2$ core leaching. It does not simply originate from the removal of the inactive $SiO_2$ from $SiO_2$@MgAl-MO.

During the furfural (F) and acetone (Ac) reactions, in addition to the main products, that is, 1,4-pentadien-3-one, 1,5-di-2-furanyl ($F_2Ac$) and 4-(2-furyl)-3-buten-2-one (FAc), an intermediate product, [4-(2-furyl)-4-hydroxy-butan-2-one (FAc-OH, $C_8$ alcohol)], was formed. This was in agreement with the commonly accepted reaction pathway for aldol condensation reaction of furfural with acetone (Smoláková et al., 2017). The selectivity versus conversion ratio of furfural toward FAc-OH, FAc, and $F_2Ac$ are presented in Fig. 9B, C, and D, respectively. Overall, with increasing furfural conversion, the selectivity to FAc and $F_2Ac$ increased, while that of FAc-OH decreased. This dependence shows that FAc-OH was an intermediate product, while FAc and $F_2Ac$ are secondary products. Moreover, for the identical furfural conversion study, almost all the tested materials showed approximately the same selectivity values. In the case of the most active catalyst (@MgAl-MO_4h), the selectivity toward FAc-OH was slightly lower, indicating a slightly better dehydration efficiency of this catalyst compared to the other tested materials. It is worth emphasising that the presence of other organic products, such as diacetone alcohol formed due to the self-condensation of acetone, cannot be excluded.

Typically, factors such as composition, acid-base properties, and textural and structural properties of the MOs influence the catalytic performance of the materials in the aldol condensation reaction (Dubnová et al., 2021; Hora et al., 2015; Kikhtyanin et al., 2018; Smolakova et al., 2018; Smoláková et al., 2017). The correlation of furfural conversion to the concentration of basic sites per gram of catalyst for all materials tested is given in Fig. 10. The linear increase of furfural conversion to the total number of basic sites concurs with the already reported critical role of number of basic sites in catalyst material on the aldol condensation reaction of furfural (Smoláková et al., 2017). A linear dependence was obtained despite the ambiguous correlation between the total number of basic sites and the Si/(Si + Mg + Al) molar ratio and for the material with chaotic morphology ($SiO_2$@MgAl-MO_ChM). On the other hand, there was no correlation between furfural conversion and the amounts of basic sites per square metre [$\mu mol \cdot m^{-2}$] or the amounts of basic sites per 1 g of MgAl phase [$\mu mol \cdot g_{MgAl}^{-1}$]. This indicates that neither a high value of specific surface area nor a high content of MgAl-MO phase alone does not ensure a high furfural conversion. Therefore, the efficiency of the core-shell catalysts in aldol condensation relies on the balance between the total number of basic sites and the morphology of the catalyst.

## 4. Conclusions

There is described a straightforward pathway for improving the morphology, textural properties, and accessibility of active sites of frequently used LDH and MO materials. Well-organised, hollow @MgAl-LDH and @MgAl-MO spheres, which were derived from $SiO_2$@MgAl-LDH core-shell hybrids, is prepared. A gradual and controlled removal of the $SiO_2$ core from $SiO_2$@MgAl-LDH (Mg/Al = 2) on NaOH solution treatment for a period of 1, 2, 4, and 6 h was established as an efficient approach.

The starting $SiO_2$@MgAl-LDH was successfully synthesised by coprecipitation with the coexistence of nonporous spherical $SiO_2$ particles uniform size and diameters of ~500 nm, as obtained previously in the modified Stöber process. The fabricated $SiO_2$@MgAl-LDH particles possess a desirable spherical shape with mainly vertically immobilized MgAl-LDH on $SiO_2$. It was shown that an increased treatment time in an alkali medium while maintaining the concentration of NaOH solution and the operating temperature, efficiently eliminated the scarified template. It is proved that @MgAl-LDH spheres formed do not collapse and hence, preserve their original spherical shape. The alkaline

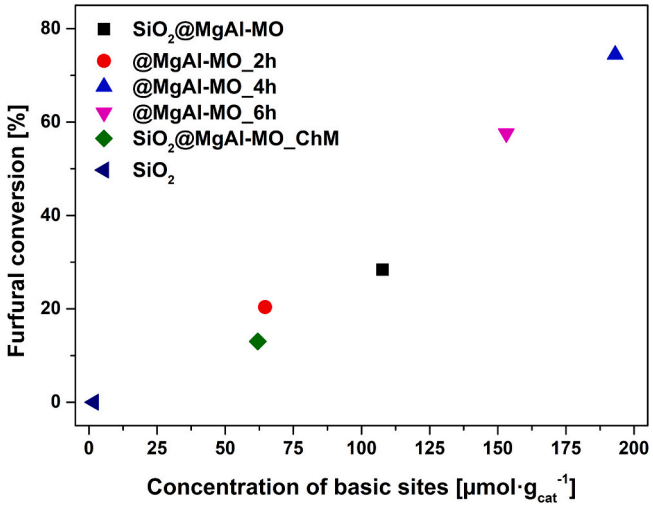


**Fig. 10.** Dependence of furfural conversion and concentration of basic sites in $\mu mol \cdot g_{cat}^{-1}$.

environment does not change the structure of the MgAl-LDH phase present in the outer layer of the core-shell systems. The gradual elimination of $SiO_2$ from $SiO_2$@MgAl-LDH resulted in materials with highly developed porosities and specific surface areas. The calcination of LDH-based materials led to the formation of appropriate MO-based catalysts. The developed catalysts exhibited the satisfactory performance in the aldol condensation of furfural and acetone. In the presence of the most effective @MgAl-MO_4h catalyst, the conversion of furfural reached 74% after 4 h of reaction. Although the furfural conversion results from a more complex contribution of structural, textural, and acid-base properties, the important role of the total amount of basic sites has been shown.

The present research provides further insight into a new generation of spherical core-shell hybrids derived from LDH-based materials with exciting features and enhanced catalytic efficiency in various processes requiring basic sites.

## Credit Author Statement

Tomasz Kondratowicz (synthesis, N2-adsorption, suggestion of hypothesis), Stanislav Slang (SEM), Lada Dubnová (TPD.-CO2, basic sites), Oleg Kikhtyaninc (aldol condensation), Petr Bělina (XRD), Libor Čapek (suggestion of hypothesis)

## Declaration of Competing Interest

The authors declare that they have no known competing financial interests or personal relationships that could have appeared to influence the work reported in this paper.

## Acknowledgment

The authors gratefully thank to the Czech Science Foundation of the Czech Republic (Project No. 19-22978S). T. Kondratowicz also thanks to European Regional Development Fund-Project “International mobility of employees of the University of Pardubice II” (No. CZ.02.2.69/0.0/0.0/18_053/0016969)”. S. Slang thanks to used infrastructure (project LM2018103).

## References

Arnal, P.M., Schüth, F., Kleitz, F., 2006. A versatile method for the production of monodisperse spherical particles and hollow particles: Templating from binary core-shell structures. Chem. Commun. 1203–1205.

Bing, W., Zheng, L., He, S., Rao, D., Xu, M., Zheng, L., Wang, B., Wang, Y., Wei, M., 2018. Insights on active sites of CaAl-hydrotalcite as a high;performance solid base catalyst toward aldol condensation. ACS Catal. 8, 656–664.
Boccalon, E., Gorrasi, G., Nocchetti, M., 2020. Layered double hydroxides are still out in the bloom: Syntheses, applications and advantages of three-dimensional flower-like structures. In: Advances in Colloid and Interface Science, p. 102284.
Bolognini, M., Cavani, F., Scagliarini, D., Flego, C., Perego, C., Saba, M., 2002. Heterogeneous basic catalysts as alternatives to homogeneous catalysts: reactivity of Mg/Al mixed oxides in the alkylation of m-cresol with methanol. Catal. Today 75, 103–111.
Čapek, L., Kutálek, P., Smoláková, L., Hájek, M., Troppová, I., Kubička, D., 2013. The effect of thermal pre-treatment on structure, composition, basicity and catalytic activity of Mg/Al mixed oxides. Top. Catal. 56, 586–593.
Chen, X., Mi, F., Zhang, H., Zhang, H., 2012. Facile synthesis of a novel magnetic core-shell hierarchical composite submicrospheres Fe3O4@ CuNiAl-LDH under ambient conditions. Mater. Lett. 69, 48–51.
Chen, C., Wang, P., Lim, T.-T., Liu, L., Liu, S., Xu, R., 2013a. A facile synthesis of monodispersed hierarchical layered double hydroxide on silica spheres for efficient removal of pharmaceuticals from water. J. Mater. Chem. A 1, 3877–3880.
Chen, C., Yee, L.K., Gong, H., Zhang, Y., Xu, R., 2013b. A facile synthesis of strong near infrared fluorescent layered double hydroxide nanovehicles with an anticancer drug for tumor optical imaging and therapy. Nanoscale 5, 4314–4320.
Chen, C., Yang, M., Wang, Q., Buffet, J.-C., O'Hare, D., 2014. Synthesis and characterisation of aqueous miscible organic-layered double hydroxides. J. Mater. Chem. A 2, 15102–15110.
Chen, C., Felton, R., Buffet, J.-C., O'Hare, D., 2015. Core–shell SiO 2@ LDHs with tuneable size, composition and morphology. Chem. Commun. 51, 3462–3465.
Chen, C., Greenwood, M., Buffet, J.-C., O'Hare, D., 2020. Aqueous miscible organic layered double hydroxides as catalyst precursors for biodiesel synthesis. Green Chem. 22, 3117–3121.
Clark, I., Smith, J., Gomes, R.L., Lester, E., 2020. Towards the continuous hydrothermal synthesis of ZnO@ Mg2Al-CO3 core-shell composite nanomaterials. Nanomaterials 10, 2052.
Creasey, J.J., Chieregato, A., Manayil, J.C., Parlett, C.M., Wilson, K., Lee, A.F., 2014. Alkali-and nitrate-free synthesis of highly active Mg–Al hydrotalcite-coated alumina for FAME production. Catal. Sci. Technol. 4, 861–870.
Di Cosimo, J., 2000. Apesteguı, amp, CŔ a, MJL Ginés and E. Iglesia. J. Catal. 190, 261–275.
Di Cosimo, J., Dıez, V., Xu, M., Iglesia, E., Apesteguıa, C., 1998. Structure and surface and catalytic properties of Mg-Al basic oxides. J. Catal. 178, 499–510.
Dou, Y., Zhang, S., Pan, T., Xu, S., Zhou, A., Pu, M., Yan, H., Han, J., Wei, M., Evans, D. G., 2015. TiO2@ Layered double hydroxide core–shell nanospheres with largely enhanced photocatalytic activity toward O2 generation. Adv. Funct. Mater. 25, 2243–2249.
Dubnová, L., Smoláková, L., Kikhtyanin, O., Kocík, J., Kubička, D., Zvolská, M., Pouzar, M., Čapek, L., 2021. The role of ZnO in the catalytic behaviour of Zn-Al mixed oxides in aldol condensation of furfural with acetone. Catal. Today 379, 181–191.
Ganesh, I., 2013. A review on magnesium aluminate (MgAl2O4) spinel: synthesis, processing and applications. Int. Mater. Rev. 58, 63–112.
Grabowska, H., Zawadzki, M., Syper, L., Mišta, W., 2005. Mg, Al-mixed oxide system: Synthesis under hydrothermal conditions, physico-chemical characterisation and application as an efficient catalyst for imidazole methylation. Appl. Catal. A Gen. 292, 208–214.
Gu, Z., Atherton, J.J., Xu, Z.P., 2015. Hierarchical layered double hydroxide nanocomposites: structure, synthesis and applications. Chem. Commun. 51, 3024–3036.
Güttel, R., Paul, M., Schüth, F., 2011. Activity improvement of gold yolk–shell catalysts for CO oxidation by doping with TiO 2. Catal. Sci. Technol. 1, 65–68.
Hora, L., Kelbichová, V., Kikhtyanin, O., Bortnovskiy, O., Kubička, D., 2014. Aldol condensation of furfural and acetone over MgAl layered double hydroxides and mixed oxides. Catal. Today 223, 138–147.
Hora, L., Kikhtyanin, O., Čapek, L., Bortnovskiy, O., Kubička, D., 2015. Comparative study of physico-chemical properties of laboratory and industrially prepared layered double hydroxides and their behavior in aldol condensation of furfural and acetone. Catal. Today 241, 221–230.
Hoyos-Castaño, D.L., Alarcón, E., Villa, A.L., 2019. Mixed oxides of hydrotalcites as catalysts for nopol epoxidation. Catal. Lett. 149, 1611–1620.
Kikhtyanin, O., Lesnik, E., Kubička, D., 2016. The occurrence of Cannizzaro reaction over Mg-Al hydrotalcites. Appl. Catal. A Gen. 525, 215–225.
Kikhtyanin, O., Čapek, L., Smoláková, L., Tisler, Z.K., Kadlec, D., Lhotka, M., Diblíková, P., KubiČka, D., 2017. Influence of Mg–Al mixed oxide compositions on their properties and performance in aldol condensation. Ind. Eng. Chem. Res. 56, 13411–13422.
Kikhtyanin, O., Čapek, L., Tišler, Z., Velvarská, R., Panasewicz, A., Diblíková, P., Kubička, D., 2018. Physico-chemical properties of MgGa mixed oxides and reconstructed layered double hydroxides and their performance in aldol condensation of furfural and acetone. Front. Chem. 6, 176.
Kikhtyanin, O., Korolova, V., Spencer, A., Dubnová, L., Shumeiko, B., Kubička, D., 2021. On the influence of acidic admixtures in furfural on the performance of MgAl mixed oxide catalysts in aldol condensation of furfural and acetone. Catal. Today 367, 248–257.
Kim, J., Lee, D., 2016. Core–shell metal–ceramic microstructures: Mechanism of hydrothermal formation and properties as catalyst materials. Chem. Mater. 28, 2786–2794.
Kondratowicz, T., Drozdek, M., Rokicińska, A., Natkański, P., Michalik, M., Kuśtrowski, P., 2019. Novel CuO-containing catalysts based on ZrO2 hollow spheres for total oxidation of toluene. Microporous Mesoporous Mater. 279, 446–455.
Kwok, W.L., Crivoi, D.-G., Chen, C., Buffet, J.-C., O'Hare, D., 2018. Silica@ layered double hydroxide core–shell hybrid materials. Dalton Trans. 47, 143–149.
Lee, H., Lee, D., 2020. Synthesis chemistry and properties of Ni catalysts fabricated on SiC@ Al2O3 core-shell microstructure for methane steam reforming. Catalysts 10, 391.
León, M., Diaz, E., Bennici, S., Vega, A., Ordónez, S., Auroux, A., 2010. Adsorption of CO2 on hydrotalcite-derived mixed oxides: sorption mechanisms and consequences for adsorption irreversibility. Ind. Eng. Chem. Res. 49, 3663–3671.
Li, R., Xue, T., Bingre, R., Gao, Y., Louis, B., Wang, Q., 2018. Microporous Zeolite@ vertically aligned Mg–Al layered double hydroxide Core@ Shell structures with improved hydrophobicity and toluene adsorption capacity under wet conditions. ACS Appl. Mater. Interfaces 10, 34834–34839.
Li, Y., Bi, H.-Y., Liang, Y.-Q., Mao, X.-M., Li, H., 2019. A magnetic core-shell dodecyl sulfate intercalated layered double hydroxide nanocomposite for the adsorption of cationic and anionic organic dyes. Appl. Clay Sci. 183, 105309.
Lyu, M., Chen, C., Buffet, J.-C., O'Hare, D., 2020. A facile synthesis of layered double hydroxide based core@ shell hybrid materials. New J. Chem. 44, 10095–10101.
Mi, F., Chen, X., Ma, Y., Yin, S., Yuan, F., Zhang, H., 2011. Facile synthesis of hierarchical core–shell Fe 3 O 4@ MgAl–LDH@ au as magnetically recyclable catalysts for catalytic oxidation of alcohols. Chem. Commun. 47, 12804–12806.
Ni, Y., Yao, L., Wang, Y., Liu, B., Cao, M., Hu, C., 2017. Construction of hierarchically porous graphitized carbon-supported NiFe layered double hydroxides with a core–shell structure as an enhanced electrocatalyst for the oxygen evolution reaction. Nanoscale 9, 11596–11604.
Nishimura, S., Takagaki, A., Ebitani, K., 2013. Characterization, synthesis and catalysis of hydrotalcite-related materials for highly efficient materials transformations. Green Chem. 15, 2026–2042.
Pan, D., Zhang, H., Fan, T., Chen, J., Duan, X., 2011. Nearly monodispersed core–shell structural Fe3O4@ DFUR–LDH submicro particles for magnetically controlled drug delivery and release. Chem. Commun. 47, 908–910.
Qu, J., Zhang, Q., Li, X., He, X., Song, S., 2016. Mechanochemical approaches to synthesize layered double hydroxides: a review. Appl. Clay Sci. 119, 185–192.
Shao, M., Ning, F., Zhao, J., Wei, M., Evans, D.G., Duan, X., 2012a. Preparation of Fe3O4@ SiO2@ layered double hydroxide core–shell microspheres for magnetic separation of proteins. J. Am. Chem. Soc. 134, 1071–1077.
Shao, M., Ning, F., Zhao, Y., Zhao, J., Wei, M., Evans, D.G., Duan, X., 2012b. Core–shell layered double hydroxide microspheres with tunable interior architecture for supercapacitors. Chem. Mater. 24, 1192–1197.
Shirotori, M., Nishimura, S., Ebitani, K., 2014. One-pot synthesis of furfural derivatives from pentoses using solid acid and base catalysts. Catal. Sci. Technol. 4, 971–978.
Shirotori, M., Nishimura, S., Ebitani, K., 2017. Fine-crystallized LDHs prepared with SiO 2 spheres as highly active solid base catalysts. J. Mater. Chem. A 5, 6947–6957.
Shirotori, M., Nishimura, S., Ebitani, K., 2018. Effect of SiO 2 amount on heterogeneous base catalysis of SiO 2@ Mg–Al layered double hydroxide. RSC Adv. 8, 28024–28031.
Silva, C.C.C., Ribeiro, N.F., Souza, M.M., Aranda, D.A., 2010. Biodiesel production from soybean oil and methanol using hydrotalcites as catalyst. Fuel Process. Technol. 91, 205–210.
Smoláková, L., Frolich, K., Kocík, J., Kikhtyanin, O., Čapek, L., 2017. Surface properties of hydrotalcite-based Zn (Mg) Al oxides and their catalytic activity in aldol condensation of furfural with acetone. Ind. Eng. Chem. Res. 56, 4638–4648.
Smolakova, L., Dubnová, L., Kocik, J., Endres, J., Daniš, S., Priecel, P., Čapek, L., 2018. In-situ characterization of the thermal treatment of Zn-Al hydrotalcites with respect to the formation of Zn/Al mixed oxide active in aldol condensation of furfural. Appl. Clay Sci. 157, 8–18.
Stöber, W., 1968. Arthur; Bohn, Ernst. Controlled Growth of Monodisperse Silica Spheres in the Micron Size Range, pp. 62–69.
Suo, H., Chen, C., Buffet, J.-C., O'Hare, D., 2018. Dendritic silica@ aqueous miscible organic-layered double hydroxide hybrids. Dalton Trans. 47, 16413–16417.
Suo, H., Duan, H., Chen, C., Buffet, J.-C., O'Hare, D., 2019. Bifunctional acid–base mesoporous silica@ aqueous miscible organic-layered double hydroxides. RSC Adv. 9, 3749–3754.
Thommes, M., Kaneko, K., Neimark, A.V., Olivier, J.P., Rodriguez-Reinoso, F., Rouquerol, J., Sing, K.S., 2015. Physisorption of gases, with special reference to the evaluation of surface area and pore size distribution (IUPAC Technical Report). Pure Appl. Chem. 87, 1051–1069.
Veloso, C.O., Pérez, C.N., de Souza, B.M., Lima, E.C., Dias, A.G., Monteiro, J.L.F., Henriques, C.A., 2008. Condensation of glyceraldehyde acetonide with ethyl acetoacetate over Mg, Al-mixed oxides derived from hydrotalcites. Microporous Mesoporous Mater. 107, 23–30.
Wang, Q., O'Hare, D., 2012. Recent advances in the synthesis and application of layered double hydroxide (LDH) nanosheets. Chem. Rev. 112, 4124–4155.
Wang, C., Ma, B., Xu, S., Li, D., He, S., Zhao, Y., Han, J., Wei, M., Evans, D.G., Duan, X., 2017. Visible-light-driven overall water splitting with a largely-enhanced efficiency over a Cu2O@ ZnCr-layered double hydroxide photocatalyst. Nano Energy 32, 463–469.
Wang, K., Huang, X., Liu, Y., Fei, W., Gu, Z., 2020. Different morphologies of SiO 2@ Mg-Al-LDH nanocomposites as catalyst for the synthesis of propylene glycol methyl ether. J. Nanopart. Res. 22, 1–14.
Wang, X., Xu, J., Song, Y., 2021. Kinetic, thermodynamic and equilibrium studies on chloride adsorption from simulated concrete pore solution by core@ shell zeolite-LTA@ Mg-Al layered double hydroxides. Appl. Clay Sci. 209, 106117.

Yu, J., Wang, Q., O'Hare, D., Sun, L., 2017. Preparation of two dimensional layered double hydroxide nanosheets and their applications. Chem. Soc. Rev. 46, 5950–5974.
Zeng, H.-Y., Xu, S., Liao, M.-C., Zhang, Z.-Q., Zhao, C., 2014. Activation of reconstructed Mg/Al hydrotalcites in the transesterification of microalgae oil. Appl. Clay Sci. 91, 16–24.
Zhang, H., Zhang, G., Bi, X., Chen, X., 2013. Facile assembly of a hierarchical core@ shell Fe 3 O 4@ CuMgAl-LDH (layered double hydroxide) magnetic nanocatalyst for the hydroxylation of phenol. J. Mater. Chem. A 1, 5934–5942.
Zhang, C., Shao, M., Zhou, L., Li, Z., Xiao, K., Wei, M., 2016. Hierarchical NiFe layered double hydroxide hollow microspheres with highly-efficient behavior toward oxygen evolution reaction. ACS Appl. Mater. Interfaces 8, 33697–33703.